Section 2
PROGRESS IN LASER FUSION

2.A Time-Resolved X-Ray Photography of Imploding Shells

Time-resolved x-ray streak photography and shadowgraphy have long been important diagnostics of dynamic high-density phenomena. Their application to studies of laser-fusion issues permits the space-time analysis of laser-accelerated foils and shells.[1,2] In this section, we describe the development of new high-resolution x-ray photographic instrumentation incorporating x-ray-sensitive, electro-optic image converter tubes,[3] specifically for the purpose of studying the temporal behavior of fusion targets imploded on the OMEGA facility. An earlier x-ray system, developed at LLE in 1977, is described in Ref. 4. Time-resolved x-ray streak photography uses electro-optic streak cameras in conjunction with x-ray imaging to record the time history of that segment of an image of the plasma centered across a slit disposed in front of the photocathode. This system permits the analysis of the high-temperature plasma, while x-ray shadowgraphy with the use of a secondary laser-produced x-ray source allows the motion of cold high-density surfaces to be recorded. These techniques are illustrated schematically in Fig. 6.

The analysis of imploding fusion targets places stringent requirements on temporal and spatial resolution and on alignment accuracy. Although the intrinsic time resolution of a streak camera is limited by the temporal dispersion of the photoelectrons,[5] most time-resolved imaging studies of nanosecond x-ray phenomena are limited by the slit-width/streak-velocity ratio. The slit width should be equal to or larger than the spatial-resolution-element size at the photocathode.

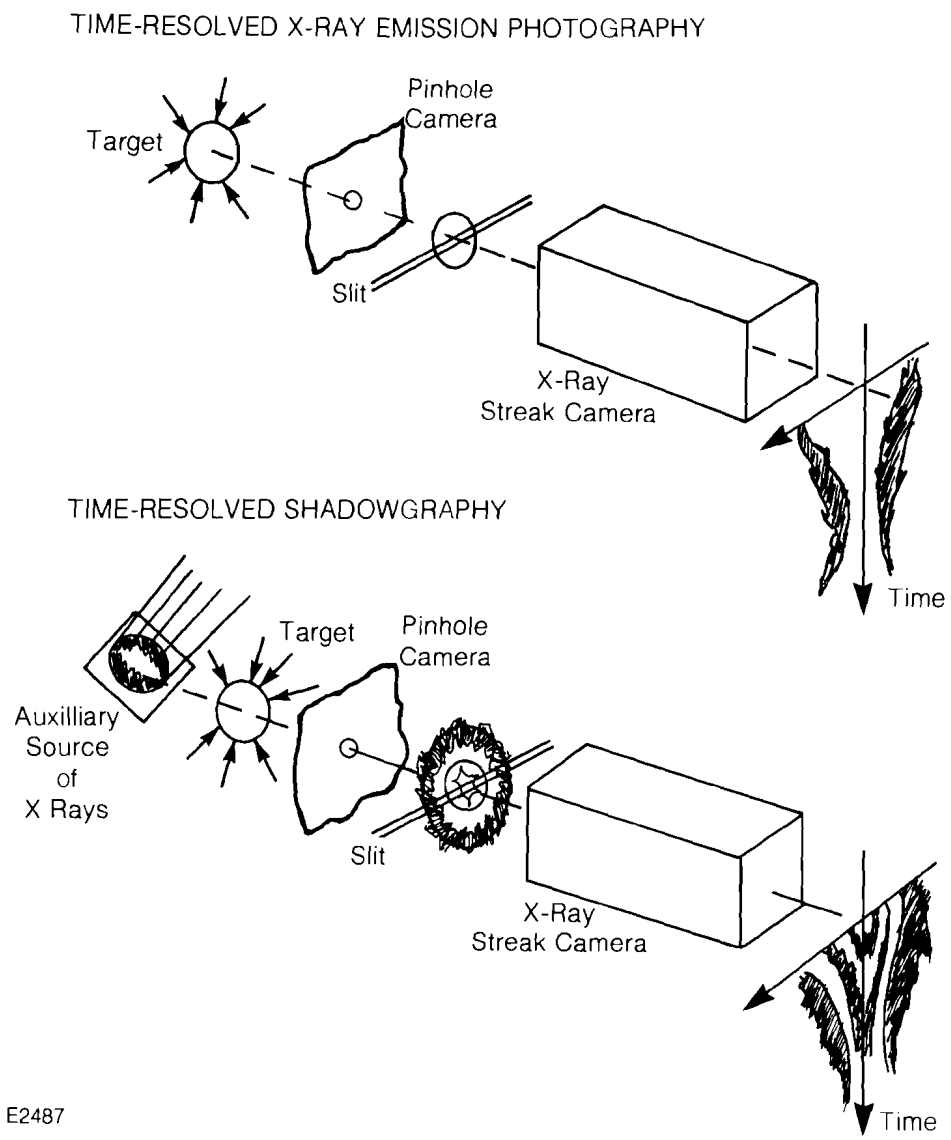

Fig. 6
General configurations for time-resolved x-ray emission photography and time-resolved shadowgraphy.

The latter, together with the number of resolution elements along the length of the slit, and the magnification and pinhole size of the imaging camera used, defines the achievable image spatial resolution. In analyzing the implosion of a spherical target, the relevant parts of the image may shrink by a factor of ~ 10 in spatial scale, and erroneous results will ensue if the slit is not positioned centrally on the final image to high accuracy ($\ll 0.1$ times the original target size). Moreover, the relevance of the resulting data to hydrodynamic simulations of target behavior is considerably increased if the streaked image is related in time to a record of the incident laser pulse, and if there is a known x-ray spectral resolution to the image. These factors are of importance to time-resolved x-ray studies of spherical targets imploded by the 24-beam OMEGA laser system.

The initial tests of this new photographic system were made with the OMEGA facility configured to provide nanosecond, 1053-nm kilojoule pulses. These conditions were required for the study of the implosions of gas-filled glass-shell targets of diameters up to 670 μm and having initial aspect ratios up to 250, under conditions of high irradiation symmetry.[6] Time-resolved photographic studies have been made with a streak pinhole camera system having high temporal and spatial resolution (20 ps and 10 μm in the target plane, respectively) and a sensitive pinhole-streak slit alignment system. In the future, this photographic system will be used for time-resolved x-ray studies of high-density implosions driven by multiple-beam, 351-nm laser light from OMEGA, and will include a temporal record of the laser pulse on the recorded streak image.

Time-Resolved Imaging System

The spherical target implosions studied with the OMEGA laser facility were of targets of initial diameter 100-500 μm. They achieved implosion velocities in excess of 10^7 cm/s and collapsed to final core dimensions of 10-60 μm, which required temporal analyses of 2- to 3-ns duration with a time resolution of ~20 ps. The system constructed for time-resolved x-ray photographic studies of these implosions incorporates a pinhole camera assembly and a custom-built x-ray streak camera. The design of the overall system is shown in Fig. 7. Images of the x-ray emission from the target region in the center of the 172-cm-diameter vacuum chamber are produced by a 7-μm pinhole on the photocathode of the streak camera, situated 70.2 cm from target, with a magnification which can be varied from 10 to 25. Thus, the image size can be optimized to the 8-mm-wide photocathode in order to use the limited number of spatial resolution elements to obtain the maximum spatial resolution in the target plane. Lateral movement of the pinhole assembly along two orthogonal axes is allowed with the strong helical flexible coupling of the pinhole assembly to the camera body with mechanical control from outside the vacuum wall. The streak camera has the basic electron-optical geometry of the Photochron II design.[7] However, considerable redesign of the individual electrostatic-field lens elements has been undertaken in order to improve stability, accuracy of alignment, and overall spatial resolution of the image-converter tube. A photograph of the streak-camera system and the pinhole camera assembly is shown in Fig. 8. Image intensification was provided by a 40-mm-diameter, electrostatically focused image intensifier, with fiber-optic coupling to the streak-tube phosphor and to the film holder.

Temporal calibration of the streak was made with the aid of the upconverted, fourth-harmonic (250-nm), single-pulse output of a mode-locked Nd:YLiF laser. This 50-ps pulse was injected into a 240-ps rattle-plate etalon which generated a train of pulses to illuminate the photocathode of the streak camera. The deflection sensitivity established from these studies was 170 ps/mm, with a linearity in the streak velocity of ~10%.

Spatial resolution in the static mode was estimated by illuminating a double-mesh structure situated immediately in front of the photo-

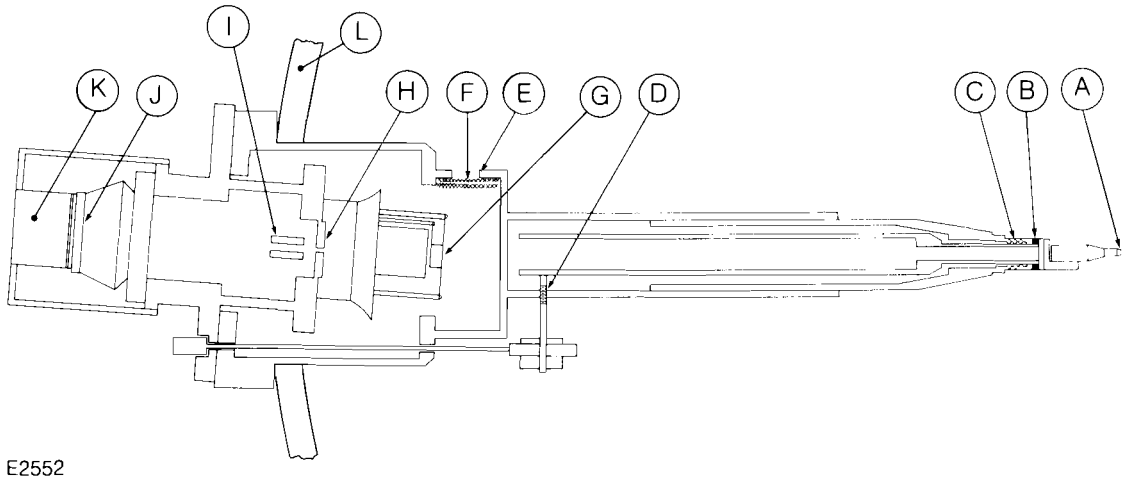

Fig. 7
Details of x-ray-imaging streak camera system. Legend: A-pinhole; B-ion deflection magnets; C-flexible coupling; D-pointing adjustment; E-streak camera pump-out port; F-ion shield; G-photocathode and acceleration grid assembly; H-anode; I-deflection electrodes; J-phosphor; K-image intensifier; L-vacuum tank wall.

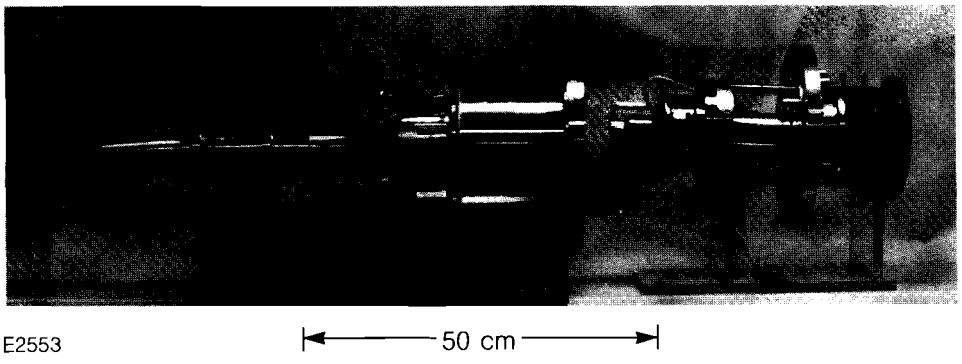

Fig. 8
Photograph of the x-ray-imaging streak camera assembly.

cathode with UV radiation from a cw D_2 lamp ($\lambda \sim 220$ nm). The coarse grid shown in Fig. 9(a) gives an indication of the degree of image distortion imposed by the electrostatic lenses in the streak tube and in the image intensifier. Within the coarse grid structure can be seen the clearly resolved fine structure (16 grid lines/mm) of the fine grid mesh [Fig. 9(b)]. This indicates that, in the static mode, the spatial resolution is somewhat better than 16 grid lines/mm. As will be seen below, this

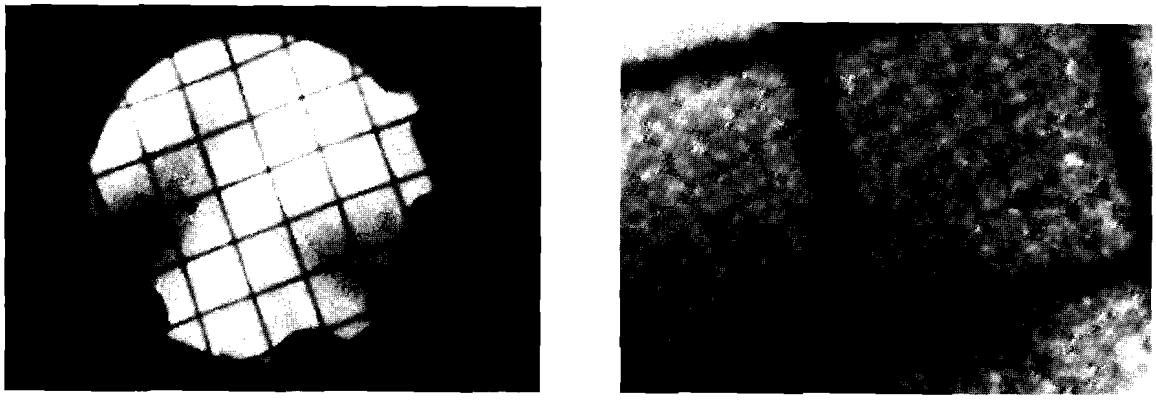

(a) Coarse Grid Spacing 1.2 mm

(b) Fine Grid Spacing 62 μm

E2554

Fig. 9
Static resolution tests of x-ray camera with UV (220-nm) radiation. (a) Coarse grid structure. (b) Resolution shown by fine grid spacing.

level of spatial resolution is maintained in the streak mode. Alignment of the system was performed with a four-axis adjustable telescope mounted on the port opposing the camera system. It was estimated that the image of the 400-μm-diameter target was centered on the slit of the streak camera to an accuracy of ~40μm.

Time-Resolved Photography of Imploding Shells

Initial time-resolved photographic studies of symmetrically irradiated targets have been made with this system. These studies have permitted an evaluation of the camera and its alignment system and have provided some interesting data which can be usefully compared to the predictions of one-dimensional hydrodynamic code simulations.

The maintenance of high spatial resolution in the streak mode is illustrated in Fig. 10. This figure shows the streaked image of a 400-μm-diameter Ti sphere, irradiated uniformly with 12 beams from the OMEGA laser system. The x-ray emission (1-3 keV) persists for the duration of the laser pulse. Distinct limb-brightening of the image occurs as a consequence of the x rays originating from a thin coronal plasma surrounding the sphere. Numerical simulations and optical diagnosis of the coronal plasma under these irradiation conditions (~2×10^{14} W/cm^2) have established that the critical-density region and the ablation surface remain almost stationary throughout the pulse.[8] The curved nature of the limb-brightened image indicates the degree of pin-cushion distortion introduced by the image intensifier. This distortion can be eliminated numerically from a digitized form of the image. Alternatively, a planar proximity-focused image intensifier can be used. Fine line structure can be seen in the image, persisting for the duration of the streak record. This results from the fine mesh used in the acceleration grid of the streak tube (80 grid lines/mm) and gives an indication of the spatial resolution in the image in the streak mode.

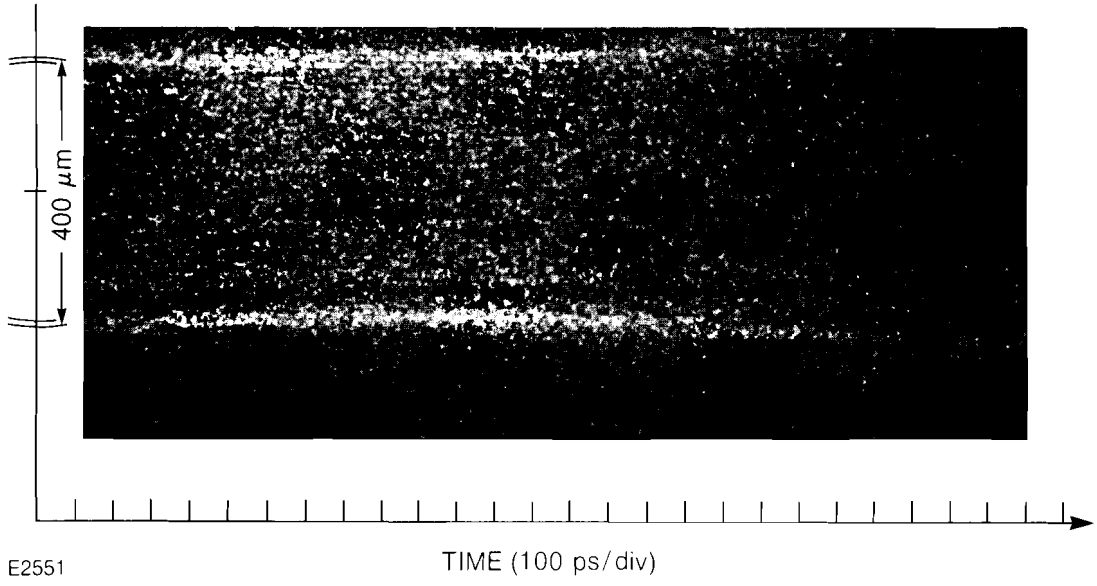

Fig. 10
Time-resolved image of the (1-3 keV) x rays emanating from a 400-μm-diameter solid Ti sphere, symmetrically irradiated by a nanosecond pulse from 12 beams of OMEGA at an intensity of 2×10^{14} W/cm².

Time-resolved images of imploding shells are shown in Fig. 11. Figure 11(a) shows the implosion of an empty 400-μm-diameter, 1.0-μm-wall, glass microballoon irradiated with 6 beams from the OMEGA system with an average intensity of $\sim1\times10^{14}$ W/cm². The x-ray image shows the symmetric compression of the shell with a maximum implosion velocity of $\sim10^7$ cm/s, with bright x-ray emission from the core of the target becoming apparent when the shell collapses on itself. The photograph shown in Fig. 11(b) is of a similarly sized target, filled with ~0.25 atm of nitrogen, irradiated at an intensity of 2×10^{14} W/cm² with a symmetric set of 12 beams of OMEGA. In this case, the initial shell radius of 200 μm is compressed with an implosion velocity above 1×10^7 cm/s, before it stagnates on the residual gas within the shell. At this point, the radius of the ablation surface is ~60 μm. Also shown in Fig. 11(b) is clear evidence of x-ray emission from within the shell. This emission occurs prior to the stagnation of the implosion and results from a shock wave, initially launched into the gas early in the implosion, impacting on the inside of the glass shell after reflection from itself at the center of the target. The continuity of the x-ray emission from this region of the target indicates that the integrity of the shell is maintained throughout the implosion. These characteristics of the implosions are in broad agreement with the predictions of one-dimensional hydrodynamic code simulations, and will be described in more detail at a later date.

Summary

We have completed the initial activation of a time-resolved x-ray imaging system to be used for photographic and shadowgraphic studies of shell implosions created by the OMEGA laser system. High temporal and spatial resolutions have been achieved and an accurate alignment system adopted. Further improvements to be incorporated

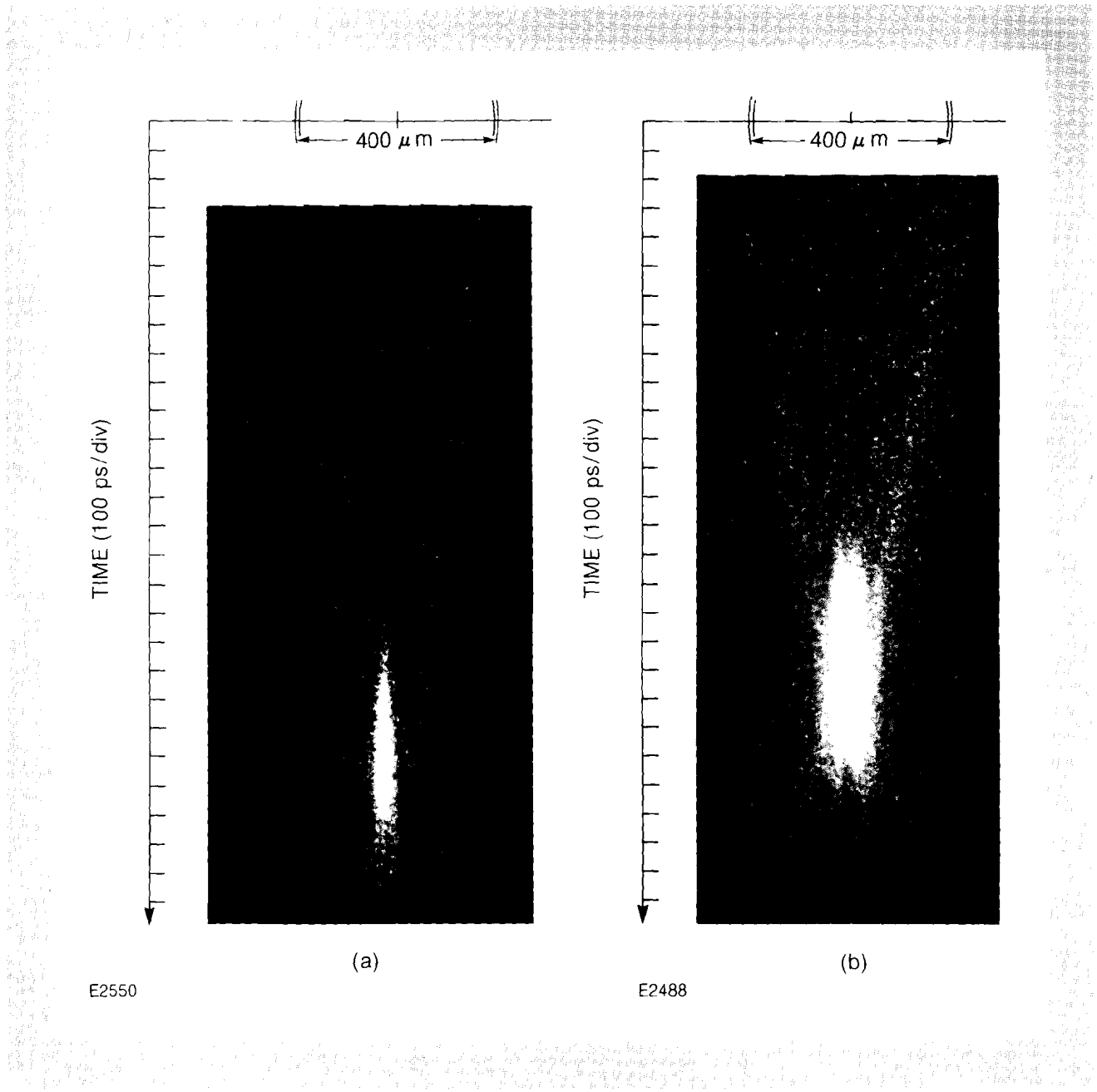

Fig. 11
Time-resolved x-ray images of (a) an empty and (b) a 0.25-atm N_2-filled glass microballoon.

into the system include the use of a proximity-focused, distortion-free image intensifier, greater x-ray spectral resolution, and the inclusion of an optical fiducial of the irradiating laser pulse. The latter will be more easily incorporated[9] for studies conducted with symmetrical arrays of up-converted 351-nm laser beams.

REFERENCES

1. D. T. Attwood, in *Proceedings of the 12th International Congress on High-Speed Photography,* edited by M. C. Richardson [*S.P.I.E.* **97**, 325 (1977)].
2. M. H. Key *et al.*, *Phys. Rev. Lett.* **41**, 1467 (1978).
3. L. W. Coleman and C. F. McConaghy, in *Proceedings of the 11th International Congress on High-Speed Photography*, edited by P. Rolls (Chapman and Hall, London, 1975), p. 196; P. R. Bird *et al.*, *ibid.*, p. 118; Yu. S. Kasyanov, A. A. Malyutin, M. C. Richardson, and V. K. Chevokin, *ibid.*, p. 561.
4. S. Letzring, Laboratory for Laser Energetics Lab Report No. 95, 1980; B. Yaakobi, D. Steel, E. Thorsos, A. Hauer, B. Perry, S. Skupsky, J. Greiger, C. M. Lee, S. Letzring, J. Rizzo, T. Mukaiyama, E. Lazarus, G. Halpern, H. Deckman, J. Delettrez, J. Soures, and R. McCrory, *Phys. Rev. A* **19**, 1247 (1979).
5. V. V. Korobkin, A. A. Malyutin, and M. Ya. Schelev, *J. Photogr. Sci.* **17**, 179 (1969).
6. M. C. Richardson, S. Skupsky, J. Kelly, L. Iwan, R. Hutchison, R. Peck, R. L. McCrory, and J. Soures, in *Proceedings of the 1983 Los Alamos Conference on Optics,* edited by R. S. McDowell and S. C. Stotlar [*S.P.I.E.* **97** (1983)].
7. P. R. Bird, D. J. Bradley, and W. Sibbett, *Proceedings of the 11th International Congress on High-Speed Photography*, edited by P. Rolls (Chapman and Hall, London, 1975), pp. 112-117.
8. M. C. Richardson *et al.*, in *Laser Interaction and Related Plasma Phenomena*, Vol. 6, edited by G. H. Miley and H. Hora (Plenum, New York, to be published 1983).
9. R. S. Marjoribanks, M. C. Richardson, J. Delettrez, S. A. Letzring, W. Seka, and D. M. Villeneuve, *Opt. Commun.* **44**, 113 (1982).

2.B Magnetic Field Effects on Electron Heat Transport

Thermal transport in laser-produced plasmas is a topic of great importance to laser fusion. In one-dimensional situations, and where moderately steep temperature gradients are believed to occur, heat fluxes considerably smaller than those predicted by the classical theories of Spitzer[1] and Braginskii[2] have been inferred experimentally. Such results are often parametrized in terms of a "flux limiter" f,[3] with the heat flux q given as a multiple f of the "free-streaming flux" q_F, defined here as $q_F = n_e kT\,(kT/m)^{1/2}$, where n_e, T, and m are the electron number density, temperature, and mass, respectively, and k is Boltzmann's constant. In two-dimensional situations, the problem is more complicated because magnetic fields generated in the laser-plasma interaction process must be considered. It is the purpose of this article to discuss some of the effects of magnetic fields on thermal transport in the presence of moderately steep temperature gradients.

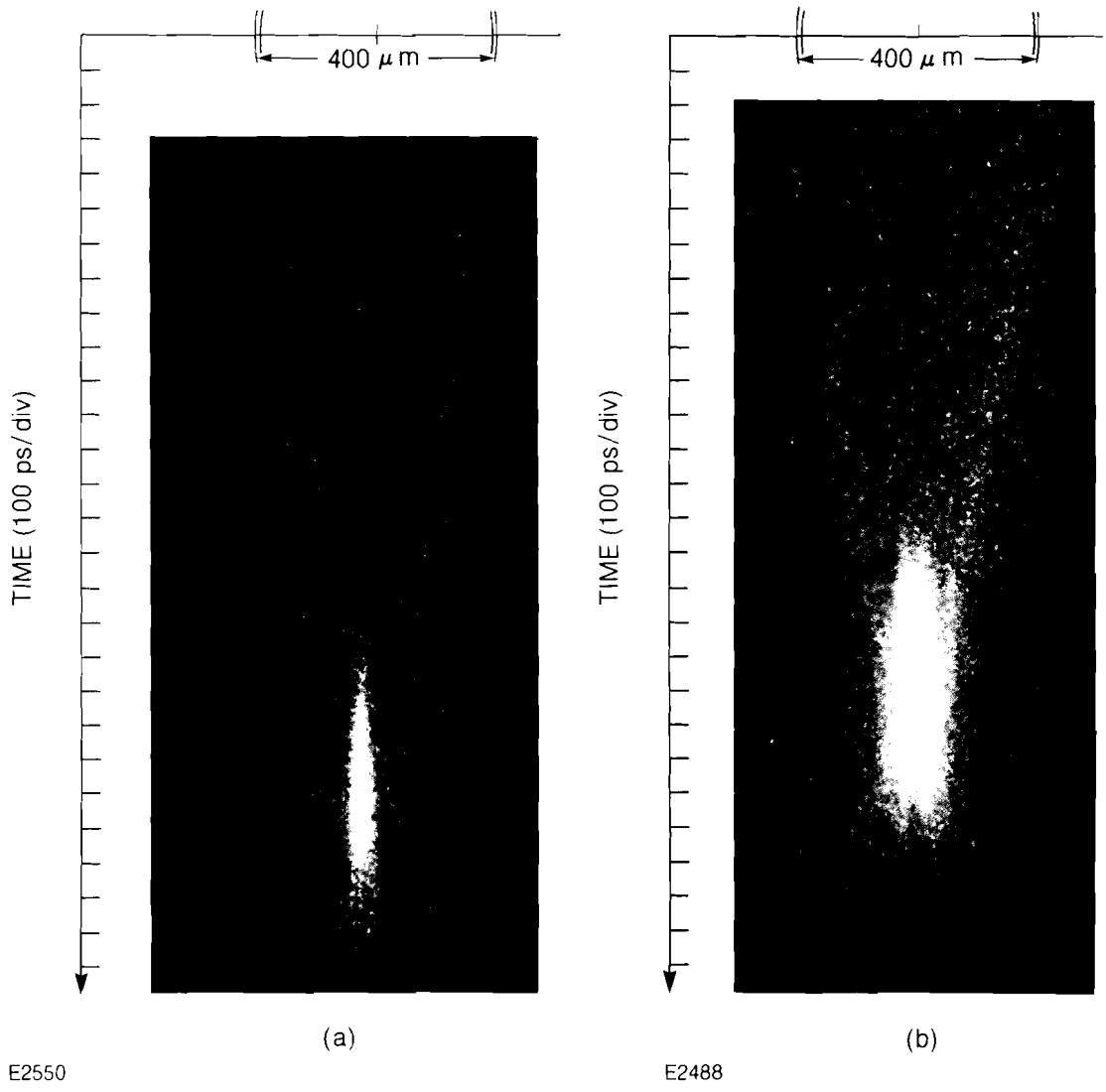

Fig. 11
Time-resolved x-ray images of (a) an empty and (b) a 0.25-atm N_2-filled glass microballoon.

into the system include the use of a proximity-focused, distortion-free image intensifier, greater x-ray spectral resolution, and the inclusion of an optical fiducial of the irradiating laser pulse. The latter will be more easily incorporated[9] for studies conducted with symmetrical arrays of up-converted 351-nm laser beams.